A Theory for Fast-Igniting Catalytic Converters

David T. Leighton and Hsueh-Chia Chang
Dept. of Chemical Engineering, University of Notre Dame, Notre Dame, IN 46556

Using asymptotic expansion and numerical analysis, we demonstrate how the step-response ignition time of an automobile catalytic converter depends on the ratio of the reaction rate to the interphase heat-transfer rate, as measured by a key Damköhler parameter χ and the degree of monolith subcooling η. In the region of low reaction rate at small χ, the normalized ignition time t_{ig} scaled by the homogeneous ignition time t_{ig}^{∞} from the inlet gas temperature is $(t_{ig}/t_{ig}^{\infty}) = 1 + 2\chi^{1/2}|ln(\chi^{1/2}/2\eta)|^{1/2}$, and the ignition takes place at a thermal front deep in the monolith. At large χ when the reaction rate is high, ignition occurs at the leading edge of the monolith with $(t_{ig}/t_{ig}^{\infty}) = 2.50 + \chi(ln\ \eta - 0.34)$. The delay in ignition time with increasing χ is due to a Taylor-Aris dispersion mechanism induced by interphase heat transfer. Although the small-χ ignition mechanism is faster, its downstream ignition location leads to a very slow upstream propagation of the thermal front that follows ignition. An optimal converter system that ignites in 13 s, 25% of the current value in a standard step-response test, is then designed by placing a small igniter, which ignites by the small-χ mechanism, upstream to preheat the current converter which then ignites by the large-χ mechanism. The length of the igniter is kept small by bypassing 2/3 of the exhaust since, from our theory, t_{ig}^{∞} is independent of the gas velocity.

Introduction

Approximately 50% of hydrocarbon and CO emissions from a light-duty automobile on an average journey occur during the "cold-start" period of about 1 min when the cold converter ignites (lights off). More stringent emission standards have rendered this performance unacceptable (Leventon, 1993) and there is an urgent need to develop fast-igniting catalytic converters in the next decade. The current ceramic monolith converter with its high efficiency under steady conditions must be redesigned to improve its startup performance. Several new designs have been proposed by Corning Inc. (Gulati et al., 1990), W. R. Grace & Co. (Whittenberger and Kubsh, 1991), Allied Signal and others (Leventon, 1993). In these new designs, the ceramic monolith converter is replaced by a metal converter with the hope of improving its heating characteristics with higher solid thermal diffusivity and lower solid thermal capacitance. However, in all these designs, it is found that the metal monoliths must still be heated at the front by a battery-driven electrical heater to significantly reduce the ignition time. The need for a new battery or an additional load on the existing battery still renders these new designs rather unattractive. There is also concern about the durability of the metal substrates (Gulati et al., 1990).

Current understanding of how the catalytic converter ignites has mostly been derived empirically or from numerical experiments (Heck et al., 1976; Young and Finlayson, 1976; Lee and Aris, 1977; Oh and Cavendish, 1982, 1983; Flytzani-Stephanopoulos et al., 1986; Zygourakis, 1989; Please et al., 1994). Oh and Cavendish of the General Motors Research Laboratories have developed a detailed numerical model and selected a set of bench mark conditions for the simulations (Oh and Cavendish, 1982, 1983). While these conditions do not correspond exactly to a current commercial converter (Oh et al., 1993), they represent a convenient base case to understand the underlying mechanisms. We shall refer to them as the "standard conditions" and adopt them for our purpose. They find that, without preheating, the standard converter ignites in about 46 s in a specific step-change experiment. They also find that this ignition time can be reduced significantly by preheating the exhaust from the standard 600 to 700 K, by reducing the cell density, by reducing the gas flow, by concentrating the catalyst loading at the front and by reducing CO poisoning with a lower CO concentration. Little improvement is found by increasing solid thermal diffusivity and unacceptable steady performance results when the

Correspondence concerning this article should be addressed to H.-C. Chang.

monolith length is reduced. Of the factors that are found to reduce the ignition time, it is unrealistic to remove CO from the exhaust or to reduce the gas flow. Varying the catalyst loading along the monolith would also be technically difficult. The effects of the cell density, which is a good design parameter, are quite complex. Decreasing cell density decreases the ignition time without preheating but increases the ignition time when the gas exhaust is preheated to 700 K. Oh and Cavendish attribute these opposite trends to a competition between the effects of gas/solid heat transfer and the solid heat capacity that is not fully understood. Based on the results of these simulations it seems likely that the only viable option for reduction in the ignition time is to preheat the converter. Indeed, this is the basis of many new converters, although some of them may not be optimally designed because of our imprecise understanding of the effects of gas flow, solid thermal diffusivity, heat capacity and porosity (cell density).

The highly exothermic oxidation reactions with high activation energies in a converter are very similar to explosive or combustive reactions. This is why there is such a clear instant of ignition when the solid temperature, after being heated from the initial cold temperature, lights off from about 600 K of the exhaust to an adiabatic temperature of about 900 K almost instantaneously at a specific location in the converter. This explosive ignition phenomenon allows us to greatly simplify the analysis of this complex behavior by reducing the kinetics to a simple zeroth-order Frank-Kamenetskii form via high-activation energy asymptotics. Because the channels in the monolith are straight to reduce pressure drop, the transport problem is also considerably simpler than a packed bed. In particular, the all-important thermal communication between the solid substrate and the gas phase and the convective heat flux in the gas phase can be reduced into an effective dispersion mechanism akin to the classical Taylor-Aris dispersion (Taylor, 1953; Aris, 1959). Here, we carry out the asymptotics using Center Manifold Theory for effective dispersion (Roberts, 1989; Balakotaiah and Chang, 1994). With these simplifications, we are able to obtain closed-form expressions for the ignition time in the limits of fast and slow reaction rates relative to the interphase heat-transfer rate which cover the range of current and future converters. These rigorously derived design equations are verified numerically and by comparison to the more complete numerical data of Oh and Cavendish. The ignition phenomena in these two limits are very distinct and their different physical mechanisms which arise from a complex interplay of thermal convection, gas/solid interaction, reaction and preheating are revealed in our analysis. The quantitative accuracy of our design equations also permits us to improve the performance of the standard converter by designing an igniter that is capable of lighting off the entire system in about 13 s without recourse to electric heating. The short igniter (one-fifth the length of the converter) introduces little additional pressure drop and can be constructed from a low thermal capacitance ceramic substrate with high (three times) but uniform catalyst loading. It hence has several advantages over electrically heated metal monoliths and still reduces the emissions during the crucial cold-start minute by 75%. This is consistent with current industrial research in this direction which has shown significant reduction in the converter light off time.

Fast-Ignition Theory

As in fast combustions and explosions (Zeldovich et al., 1985), the high activation energies of the oxidation reactions in a catalytic converter imply that the reaction rate is very sensitive to a temperature increase. The incremental temperature required to increase the rate by a factor of e is known as the Frank-Kamenetskii temperature β^{-1} and under the standard conditions of Table 1 from Oh and Cavendish, $\beta^{-1} \sim 39.5$ K, as we shall subsequently derive. This small β^{-1} indicates that ignition is a very rapid process such that before ignition and during the short ignition period, the reactant consumption is negligible. It permits us to ignore the complex kinetics for the hydrocarbons, NO, CO, O_2, H_2 and so on, and focus only on the thermal evolution that leads to ignition. This standard approximation in combustion theory, which sets all reactant concentrations to the feed conditions C_g^{in} of Table 1, can be rigorously justified (Kasoy and Liñan, 1978). For a catalytic converter, additional consideration is necessary before we can use the inlet concentrations in all our thermal dynamics. The gas reactants adsorb onto a thin coating of catalytic material where appreciable reaction takes place if the solid temperature is sufficiently high. The gas temperature, on the other hand, must heat up the entire monolith and not just the catalytic coating. The relatively small solid capacitance for the reactants implies that the surface concentration equilibrates with the gas phase much more rapidly than the surface temperature. If there is little consumption by reaction, as is the case prior to ignition, the local surface concentration can then be assumed to be equal to the local gas-phase concentration after proper correction for the area/volume factors. Also because the mass capacitance is so much lower than the heat capacitance, the concentration fronts that are established at the leading edge of the monolith when it is first exposed to the exhaust travel through the channels at a velocity close to the average gas velocity U in the channels. In contrast, we shall show that the thermal front travels with a far smaller (by three orders of magnitude) velocity U_{eff} due to the large thermal capacitance. As a result, as far as the thermal dynamics is concerned, the concentration fronts have long passed through the channels and the gas and surface concentrations have all equilibrated to the inlet values since the solid temperature is still too low to consume an appreciable fraction of the reactants. These zero consumption and fast gas/solid concentration equilibration approximations reduce the complex kinetics to an effective zeroth-order reaction in the thermal balance equation for the solid

$$2\pi a\Delta r(\rho c_p)_s \frac{\partial T_s}{\partial t} = 2\pi a h(T_g - T_s) + (2\pi a\Delta r + \pi a^2) \sum_{i=1}^{5} (-\Delta H)_i R_i\left(C_g^{in}, T_s\right) \quad (1)$$

where, as Oh and Cavendish have done, we have approximated the square channels of the monolith by cylindrical ones with radius a. We have also adopted their convention of expressing the reaction rate in a per volume monolith basis such that the feed concentrations can be used directly. In the Appendix, we show that the proper heat-transfer coefficient h

Table 1. Standard Condition*

$W = 40$ g/s	$(\rho c_p)_g = 6.3\times10^{-4}$ J/K·cm^3
$U = 1.68\times10^3$ cm/s	$(\rho c_p)_s = 2.678$ J/K·cm^3
$L = 10$ cm	$k_g = 4.7\times10^{-4}$ J/K·s·cm
$\epsilon = 0.6836$	$\alpha_g = 0.74$ cm^2/s
$\Delta z = 0.013$ cm	$\alpha_s = 6.2\times10^{-3}$ cm^2/s
$a = R_h = 0.06062$ cm	$\alpha_{\text{eff}} = 1.65$ cm^2/s
$T_s^o = 300$ K	$\gamma = 2.0\times10^3$
$T_g^{\text{in}} = 600$ K	$\chi = 0.13$
$U_{\text{eff}} = 0.86$ cm/s	$A = 1.96$
$\eta = 7.59$	$\beta = 0.0253$
$t_{ig}^{\infty} = 17.1$ s	$n = 46.5$ cells/cm^2
$L_{ig} = 13.24$ cm	$L_{\infty} = 14.7$ cm
$A_c = 60$ cm^2	

$$C_g^{\text{in}} = \begin{cases} 2\%\ \text{CO} \\ 450\ \text{ppm}\ C_3H_6 \\ 50\ \text{ppm}\ CH_4 \\ 0.667\%\ H_2 \\ 5\%\ O_2 \\ 550\ \text{ppm NO} \end{cases}$$

*Kinetics and heats of reaction are given in Oh and Cavendish (1982, 1983).

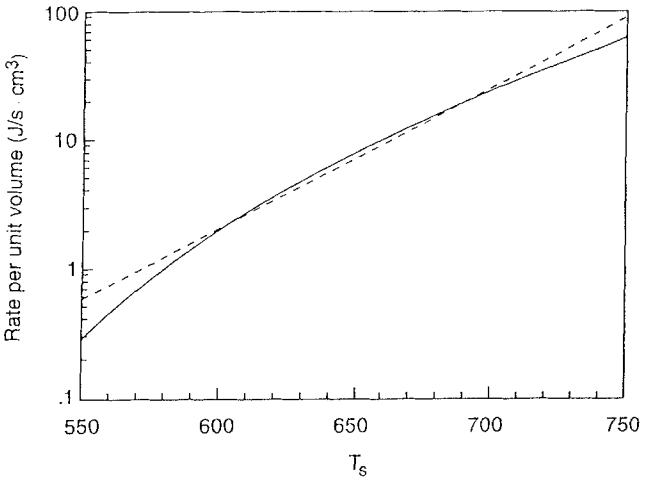

Figure 1. Zeroth-order kinetics expression (----), $Ae^{\beta(T_s - T_g^{\text{in}})}$, vs. full heat release rate (——), $\Sigma_{i=1}^{5}(-\Delta H_i)R_i(C_g^{\text{in}}, T_s)$, at standard feed conditions.

for laminar Poiseuille flow in a cylinder should be derived by imposing a constant heat flux at the wall, such that

$$h = \frac{24}{11}\left[\frac{\alpha_g(\rho c_p)_g}{a}\right]\left(\frac{\gamma}{1+\gamma}\right) \tag{2}$$

This is true when the solid wall is thin and when the heat capacity ratio

$$\gamma = \frac{2\pi a\Delta r(\rho c_p)_s}{\pi a^2(\rho c_p)_g} = \frac{(\rho c_p)_s}{(\rho c_p)_g}\left(\frac{1-\epsilon}{\epsilon}\right) \tag{3}$$

is large which are very good assumptions for a catalytic converter (see Table 1). The parameter ϵ in Eq. 3 is the monolith void fraction. A heat-transfer coefficient formulation allows us to ignore the details of the flow and heat transfer in the radial direction and use a pseudo-one-dimensional model, such as Eq. 1, instead. As is demonstrated in Appendix 1, for large γ the exact geometry of the solid walls has little effect on the heat-transfer process. Rather, the only significant effect is the ratio of the total solid heat capacity to that of the gas, which is captured in the parameter γ. This is why approximating the actual geometry, which may be quite complex in the case of metal monoliths, with a cylindrical channel is so robust.

The indices i in Eq. 1 refer to CO, C_3H_6, CH_4, H_2 and O_2, respectively. Using the kinetic parameters in Oh and Cavendish (1982, 1983), we are able to fit the zeroth-order kinetics by

$$\sum_{i=1}^{5}(-\Delta H_i)R_i\left(C_g^{\text{in}}, T_s\right) \sim Ae^{\beta(T_s - T_g^{\text{in}})} \tag{4}$$

where the exponents have essentially been expanded about the gas inlet temperature of $T_g^{\text{in}} = 600$ K to yield $A = 1.96$ J/s·cm^3 and an inverse Frank-Kamenetskii temperature of $\beta = 0.0253$ K^{-1}. As shown in Figure 1, approximation Eq. 4, which will greatly simplify our analysis, is within 20% in the range of 600 to 725 K. Actually, for ignition from 600 K, the kinetics only needs to be accurate up to 679 K when the reaction rate is e^2 times the initial. The estimate in Eq. 4 is within 10% for this important range. Beyond 725 K, the reaction is so rapid that an accurate estimate of the kinetics is unnecessary if one is only interested in the ignition phenomenon. We have also neglected thermal diffusivity in Eq. 1, which will be subsequently justified.

With these simplifications, the pertinent thermal balance equations for the gas and solid phases are

$$\pi a^2(\rho c_p)_g\left[\frac{\partial T_g}{\partial t} + U\frac{\partial T_g}{\partial x}\right] = 2\pi ah(T_s - T_g) \tag{5}$$

$$2\pi a\Delta r(\rho c_p)_s\frac{\partial T_s}{\partial t} = 2\pi ah(T_g - T_s) + (2\pi a\Delta r + \pi a^2)Ae^{\beta(T_s - T_g^{\text{in}})} \tag{6}$$

with initial and boundary conditions

$$T_g(x,0) = T_s(x,0) = T_s^0 \quad x > 0 \tag{7}$$

$$T_g(0,t) = T_g^{\text{in}} \quad t \geq 0 \tag{8}$$

It is instructive to define certain characteristic lengths and times to nondimensionalize and simplify the above equations. We use the limit of infinitely fast interphase communication as the reference point. In this limit, the convection and accumulation terms are negligible compared to the interphase transport term in both Eqs. 5 and 6. As a result, $T_s \sim T_g$ as the two temperatures equilibrate rapidly. This then allows us to combine both equations in this limit to yield

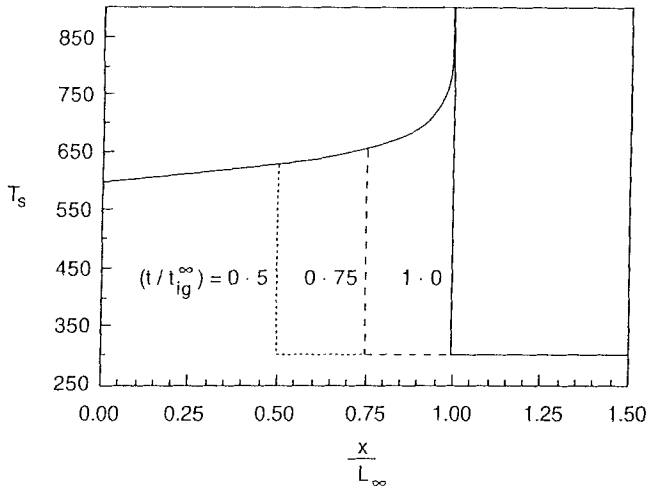

Figure 2. Ignition of the solid and gas temperatures in the limit of infinite interphase communication.

Blowup occurs at $x = L_\infty$ when $(t/t_{ig}^{\infty}) = 1$. The profiles at $(t/t_{ig}^{\infty}) = 0.5$ and 0.75 are also shown.

$$\frac{\partial T_s}{\partial t} + U_{\text{eff}} \frac{\partial T_s}{\partial x} = \frac{(2\pi a \Delta r + \pi a^2)}{(1+\gamma)\pi a^2 (\rho c_p)_g} A e^{\beta(T_s - T_g^{\text{in}})} \tag{9}$$

where

$$U_{\text{eff}} = \frac{U}{1+\gamma} \tag{10}$$

is the familiar thermal wave speed analogous to the concentration wave speed in high-affinity chromatography theory (Amundson and Aris, 1973). Due to the large heat capacity of the monolith, the wave speed is much slower than the average velocity U of the gas phase. The gas velocity is given by $U = W/A_c \epsilon \rho_g$ where ϵ is porosity, W is the mass-flow rate, A_c is the frontal area of the converter and ρ_g is the gas density. Hence, a thermal shock wave shown in Figure 2 is established by the initial and boundary conditions of Eqs. 7 and 8 and it propagates downstream at the speed of U_{eff} in the limit of infinitely fast interphase interaction. Immediately behind the shock, the temperature evolution of a point moving with speed U_{eff} is given by

$$\frac{dT_s}{dt} = \frac{e^{\beta(T_s - T_g^{\text{in}})}}{\beta t_{\text{ig}}^{\infty}} \tag{11}$$

where

$$t_{\text{ig}}^{\infty} = \frac{(1+\gamma)\pi a^2 (\rho c_p)_g}{(2\pi a \Delta r + \pi a^2) A \beta} = \frac{(1+\gamma)\epsilon (\rho c_p)_g}{A\beta}$$

$$\sim \frac{\gamma \epsilon (\rho c_p)_g}{A\beta} = \frac{(1-\epsilon)(\rho c_p)_s}{A\beta} \quad \text{at large } \gamma \tag{12}$$

Equation 11 essentially describes the temperature evolution of a monolith with spatially uniform temperature distribution which begins at T_s^0. The ignition time t_{ig}^{∞} will be called the homogeneous ignition time. A simple integration of Eq. 8 yields the behavior of Figure 2 which shows that T_s of a monolith with infinite interphase communication also blows up in finite time at t_{ig}^{∞}. This blowup to infinity is the ignition phenomenon of interest, and it occurs because of our zeroth-order kinetic simplification. In a real converter, finite reactant consumption will arrest the temperature blowup and, from Oh and Cavendish's numerical experiment, saturate it at the adiabatic temperature rise of 300 K ($T_s = T_g = 900$ K for $T_g^{\text{in}} = 600$ K for the standard conditions in Table 1). Our model hence breaks down after the ignition, but it provides a good estimate of the ignition time. In this limit of infinite interphase interaction, the ignition occurs at the ignition length

$$L_\infty = U_{\text{eff}} t_{\text{ig}}^{\infty} \tag{13}$$

The objective of our theory is to show how the ignition t_{ig} increases from t_{ig}^{∞} as the thermal communication between the phases decreases. In the limit of strong but finite interphase communication or slow reaction rate we shall show in the next section that the sharp front of Figure 2 is smoothed by an effective Taylor-Aris dispersion phenomenon due to imperfect communication, and the associated effective thermal diffusivity is given by

$$\alpha_{\text{eff}} = \left(\frac{\pi a^2 (\rho c_p)_g}{2\pi a h}\right)\left(\frac{\gamma^2}{1+\gamma}\right) U_{\text{eff}}^2 \sim \frac{11}{48}\frac{U^2 a^2}{\alpha_g \gamma} \quad \text{for } \gamma \gg 1 \tag{14}$$

Under the standard conditions of Table 1, this apparent dispersion is $\alpha_{\text{eff}} = 1.65$ cm^2/s which is significantly larger than the typical solid thermal diffusivity 6.2×10^{-3} of a ceramic monolith or even 0.6 cm^2/s of a metal monolith (Gulati et al., 1990). This shows that solid thermal diffusivity is unimportant in the ignition phenomenon and can be safely omitted.

Using α_{eff} without fully understanding its origin for now, we define the key dimensionless parameter χ of the problem:

$$\chi = \frac{\alpha_{\text{eff}}}{U_{\text{eff}}^2 t_{\text{ig}}^{\infty}} \tag{15}$$

which measures the ratio of axial dispersion to axial convection during the characteristic time for ignition t_{ig}^{∞}. Since the distance the thermal front propagates into the monolith prior to ignition scales as $U_{\text{eff}}\, t_{\text{ig}}^{\infty}$, while the length scale for dispersion scales as $(\alpha_{\text{eff}} t_{\text{ig}}^{\infty})^{1/2}$, the importance of dispersion decreases with increasing t_{ig}^{∞}. Thus, a high reaction rate (small t_{ig}^{∞}) actually increases the importance of axial dispersion in delaying the ignition. An alternative interpretation for the parameter χ may be obtained if we substitute the expressions for U_{eff}, t_{ig}^{∞}, and α_{eff} at large γ (Eqs. 10, 12, and 14) into Eq. 15,

$$\chi \approx \frac{A\beta}{\epsilon}\frac{11}{48}\frac{a^2}{k_g} \quad \text{for } \gamma \gg 1 \tag{16}$$

from which it is seen that χ may be regarded as a modified group IV Damköhler number, the ratio of the reaction rate to radial diffusion through the gas phase. We note that since α_{eff} scales as U^2, χ is independent of U. One can actually reduce the gas velocity to reduce the length of the converter without changing the ignition time! This observation will become important in our design of a better converter.

Let $t_c = \alpha_{\text{eff}}/U_{\text{eff}}^2 = t_{\text{ig}}^{\infty}\chi$ be the characteristic timescale and $x_c = \alpha_{\text{eff}}/U_{\text{eff}} = L_{\infty}\chi$ the characteristic length scale which result between a balance of dispersion and convection and let $u = \beta(T_g - T_g^{\text{in}})$ and $v = \beta(T_s - T_g^{\text{in}})$ be the dimensionless gas and solid temperatures, respectively. The original thermal Eqs. 5 and 6 and conditions 7 and 8 can be scaled to:

$$\frac{1}{\gamma}\frac{\partial u}{\partial \tau} + \frac{\partial u}{\partial y} = v - u \tag{17}$$

$$\frac{\partial v}{\partial \tau} = u - v + \chi e^{v} \tag{18}$$

$$u(y,0) = v(y,0) = -\eta \quad y \geq 0 \tag{19}$$

$$u(0,\tau) = 0 \quad \tau \geq 0 \tag{20}$$

in the limit of large γ where

$$\eta = \beta\left(T_g^{\text{in}} - T_s^0\right) > 0 \tag{21}$$

$$y = x/x_c = x/(L_{\infty}\chi) \tag{22}$$

$$\tau = t/t_c = t/(t_{\text{ig}}^{\infty}\chi) \tag{23}$$

There are hence 3 parameters in the system: γ, χ and η. However, since the solid thermal capacity is so much larger than that of gas ($\gamma \gg 1$), the term of $O(\gamma^{-1})$ will be shown subsequently to be negligible. Note, however, the remaining two parameters are still functions of γ as γ approaches infinity due to the dependence of t_{ig}^{∞}, α_{eff} and U_{eff} on γ. The parameter η measures the degree of preheating or subcooling (the difference between inlet gas temperature and cold substrate temperature) normalized by the Frank-Kamenetskii temperature β^{-1}. Values of χ and η for the standard converter are listed in Table 1.

Slow Reaction Limit ($\chi \ll 1$)

In the limit of slow reaction, we shall derive the proper equation that describes the Taylor-Aris dispersion that arises due to imperfect heat transfer between the phases. In the classical Taylor-Aris dispersion of a solute, the dispersion arises because finite radial diffusion in a pipe lands different particles at the same axial position on streamlines with different speeds and, hence, after some initial transient, there is a net axial separation of the solute particles that can be described by an effective diffusion process. An interesting aspect of this apparent axial dispersion process due to a coupling between radial diffusion and axial velocity gradient is that it decreases with increasing radial diffusion and increases with increasing axial flow. The former smooths the radial concentration gradient while the latter increases it. In quantitative terms, the effective dispersion scales as the square of the Peclet number (Taylor, 1953).

In the present converter problem, effective axial solute dispersion of the classical problem is replaced by thermal dispersion. The large heat capacity of the stationary phase (large γ) leads to the axial dispersion being dominated by the difference in velocity between the mobile gas and stationary wall rather than any velocity gradient in the gas phase. If interphase heat transfer is not strong enough, this velocity difference establishes a normal thermal gradient which, in turn, introduces an effective thermal dispersion in the axial direction. Another physical visualization is to consider this mechanism to arise because the solid temperature does not equilibrate instantaneously with the gas temperature, such that the solid thermal shock lags behind the gas shock. This interphase gradient causes a smoothing of the shock structures in both phases that resembles an apparent axial diffusion smoothing. It is this Taylor-Aris smoothing that reduces the thermal front temperature and delays the ignition process. We shall rigorously derive the thermal dispersion mechanism here and estimate its effect on the ignition time in the limit of small χ. The Taylor-Aris dispersion mechanism exists for all values of γ and, in fact, a relative order between χ and γ does not need to be specified. However, the heat capacity ratio γ of a catalytic converter is large and this results in a simpler effective equation that describes the dispersion.

The relaxation time of the gas-phase temperature is of order $\tau \sim \gamma^{-1}$ from Eq. 17 and the solid thermal time scale of order unity from Eq. 18. Since Taylor-Aris dispersion is established when the temperatures of both phases are equilibrated, it makes sense to define a new time scale $\theta = \gamma\tau$ in this limit of slow reaction such that the equilibration occurs within unit order in θ. In the limit of small χ, dispersion is weak and the characteristic length for ignition to occur is simply $L_{\infty} = U_{\text{eff}} t_{\text{ig}}^{\infty}$ of Eq. 13. Hence, a new spatial coordinate $z = \chi y = x/L_{\infty}$ should be defined in this limit. The new characteristic time $t_{\text{ig}}^{\infty}\chi/\gamma$ and length L_{∞} used here for the weak dispersion limit, when convection and reaction balance, then replaces t_c and $L_{\infty}\chi$ in Eqs. 17 and 18 when dispersion and convection balance. In the new variables, Eqs. 17 and 18 become

$$\frac{\partial u}{\partial \theta} = v - u - \chi\frac{\partial u}{\partial z} \tag{24}$$

$$\frac{\partial v}{\partial \theta} = \frac{1}{\gamma}(u - v) + \frac{\chi}{\gamma}e^{v} \tag{25}$$

which can be rewritten as

$$\frac{\partial}{\partial \theta}\begin{pmatrix} u \\ v \end{pmatrix} = \begin{pmatrix} -1 & 1 \\ 1/\gamma & -1/\gamma \end{pmatrix}\begin{pmatrix} u \\ v \end{pmatrix} + \chi\begin{pmatrix} -\dfrac{\partial u}{\partial z} \\ \gamma e^{v} \end{pmatrix} \tag{26}$$

The last vector contains small terms in the region when Taylor-Aris dispersion has developed. A similarity transform

$$\begin{pmatrix} u \\ v \end{pmatrix} = \begin{pmatrix} 1 & 1 \\ 1 & -1/\gamma \end{pmatrix}\begin{pmatrix} w_1 \\ w_2 \end{pmatrix}$$

yields

$$\frac{\partial}{\partial\theta}\begin{pmatrix} w_1 \\ w_2 \end{pmatrix} = \begin{pmatrix} 0 & 0 \\ 0 & -1-\dfrac{1}{\gamma} \end{pmatrix} - \chi \begin{pmatrix} \dfrac{1}{1+\gamma}\dfrac{\partial w_1}{\partial z} + \dfrac{1}{1+\gamma}\dfrac{\partial w_2}{\partial z} - \dfrac{1}{1+\gamma}e^{w_1-w_2/\gamma} \\ \dfrac{\gamma}{1+\gamma}\dfrac{\partial w_1}{\partial z} + \dfrac{\gamma}{1+\gamma}\dfrac{\partial w_2}{\partial z} + \dfrac{1}{1+\gamma}e^{w_1-w_2/\gamma} \end{pmatrix} \quad (27)$$

In this form, it is clear that $w_2 = \gamma/(1+\gamma)(u-v)$ decays very rapidly in the time with a decay rate of approximately -1, the characteristic time for the temperatures to equilibrate. In fact, a vanishingly small w_2 corresponds to perfect equilibration between the solid and gas temperatures $u - v = w_2 = 0$. We are, in fact, interested in the case when w_2 does not vanish completely, viz. when the interphase communication is imperfect. One can use the Center Manifold Theory (Balakotaiah and Chang, 1994; Roberts, 1989) to resolve this limit. In Eq. 27, the terms in the final bracket are of order χ. Hence, to leading order, the dynamics of w_1 and w_2 are associated with eigenvalues of zero and -1, respectively. As time θ advances to unit order, w_2 is small relative to w_1 but its evolution is much faster than that of w_1. This asymptotic evolution of w_2 is "adiabatically" coupled to w_1 through the second equation in Eq. 27. This coupling can be obtained through the Center Manifold Theory or simply by invoking a standard quasi-steady-state approximation on the w_2 equation in Eq. 27. The result to leading order is

$$w_2 \sim -\frac{\gamma^2\chi}{(1+\gamma)^2}\frac{\partial w_1}{\partial z} \quad (28)$$

where the $\partial w_1/\partial z$ and the reaction term in the equation do not contribute to this leading order expression. Substituting this expression into the first equation in Eq. 27, one obtains the following effective reaction-convection diffusion equation

$$\frac{\partial w_1}{\partial\theta} + \frac{\chi}{1+\gamma}\frac{\partial w_1}{\partial z} = \frac{\gamma^2\chi^2}{(1+\gamma)^3}\frac{\partial^2 w_1}{\partial z^2} + \frac{\chi}{1+\gamma}e^{w_1-w_2/\gamma} \quad (29)$$

where $w_1 = u/(1+\gamma) + [\gamma/(1+\gamma)]v$ is capacitance-weighted average temperature between the phases. It is this average temperature that is described by an effective reaction-convection-diffusion equation. It is clear that, regardless of the value of γ, convection balances with reaction in this small χ limit and dispersion enters in the next order. In the limit of large γ for a catalytic converter, $w_1 \sim v$ is simply the solid temperature and Eq. 29 reduces to

$$\frac{\partial v}{\partial\theta} + \frac{\chi}{\gamma}\frac{\partial v}{\partial z} = \frac{\chi^2}{\gamma}\frac{\partial^2 v}{\partial z^2} + \frac{\chi}{\gamma}e^v \quad (30)$$

If the higher-order dispersing term is neglected, one obtains in terms of the original variables

$$\frac{\partial v}{\partial\tau} + \frac{\partial v}{\partial y} = \chi e^v \quad (31)$$

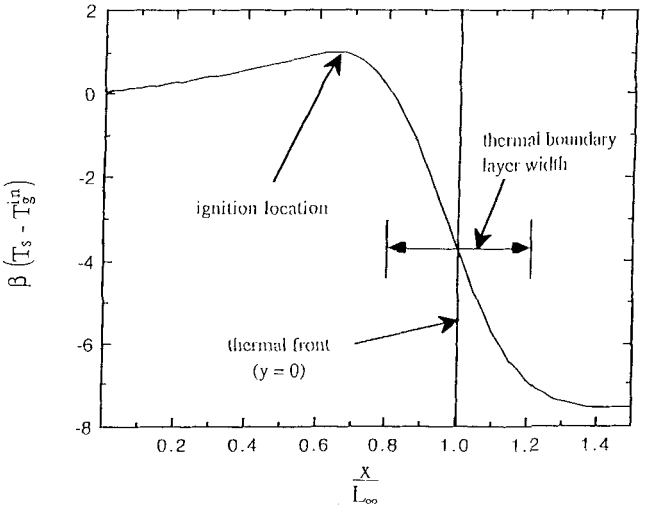

Figure 3. Solid temperature distribution when $\chi = 0.01$ is small but nonzero and $\eta = 7.59$.

The distribution is at $(t/t_{ig}^{\infty}) = 1$. Comparing to Figure 2, one sees that the sharp front at the Lagrangian coordinate of $y = 0$ has been smoothed and a thermal diffusion boundary layer appears.

which is simply a dimensionless version of Eq. 9. From this dispersionless leading-order version, which corresponds to infinitely fast heat transfer, the initial conditions 19 stipulate that a square shock wave with unit speed traverses the converter, as shown in Figure 2. A point immediately behind the shock, which has remained in the converter longer than any other point in the elevated portion of the shock, ignites first at $t_{ig} = t_{ig}^{\infty}$ or $\tau_{ig}^{\infty} = \chi^{-1}$ in the original dimensionless variable. However, Eq. 30 indicates that with the apparent Taylor-Aris dispersion term, the shock will be smoothed and the ignition time delayed. This delayed ignition is described by Eq. 30 or, in the original variables:

$$\frac{\partial v}{\partial\tau} + \frac{\partial v}{\partial y} = \frac{\partial^2 v}{\partial y^2} + \chi e^v \quad (32)$$

and we shall use this equation to study how the ignition time is delayed from $\tau_{ig}^{\infty} = \chi^{-1}$ due to dispersion at this small χ limit.

The unit dispersion coefficient in the new-found dispersion term of Eq. 32 indicates that α_{eff} in Eq. 14 is the correct dispersion coefficient for the solid temperature that results due to imperfect interphase communication. The appearance of a second-order derivative in y necessitates conditions other than Eq. 19 which will be discussed subsequently. It is, however, important to emphasize that the origin of this apparent dispersion term is due to coupling between imperfect interphase communication and the gradient between the gas and solid convection velocities. As such, the upstream thermal feedback implied in the diffusion term is completely artificial. A pulse of temperature will not diffuse in the negative y direction as predicted by Eq. 32, since there is no such mechanism in the original Eqs. 17 and 18. However, the smearing shown in Figure 3, which is due to downstream separation, is accurately described by Eq. 32.

For χ small, as we have assumed in deriving Eq. 32, and after an initial transient of $\tau \sim O(\gamma^{-1})$, a front is established which travels downstream with unit velocity in the $y-\tau$ space. The actual front travels at a speed of U_{eff} of Eq. 10 in reality. We hence get on a Lagrangian frame which moves with the front such that Eq. 32 becomes

$$\frac{\partial \upsilon}{\partial \tau} = \frac{\partial^2 \upsilon}{\partial y^2} + \chi e^{\upsilon} \tag{33}$$

Far behind the front, the solid temperature υ should approach the inlet gas temperature $u = 0$ since it has had time to equilibrate, whereas far in front the solid temperature remains at the initial value of $-\eta$. Hence, the appropriate boundary conditions for the above diffusion-reaction equation are

$$\lim_{y \to -\infty} \upsilon = 0 \qquad \lim_{y \to +\infty} \upsilon = -\eta \tag{34}$$

For small χ, the reaction term is unimportant initially and one has a simple diffusion problem from a step function in the Langrangian frame. This apparent diffusion creates a thermal diffusion boundary layer of thickness $y \sim O(2\sqrt{\tau})$, as shown in Figure 3. This diffusion boundary layer removes the possibility of igniting right behind the front $y = 0^-$ in the Lagrangian frame as in Figure 2 for the case of infinitely fast interphase communication. Ignition will instead occur at a point $y_{\text{ig}} < 0$ behind the diffusive boundary layer and hence requires a longer time, since the new ignition point y_{ig} has not been in the converter as long as the point $y = 0^-$, as shown in Figure 3. Since the ignition at y_{ig} is very localized, away from a small neighborhood of y_{ig} the solid temperature υ evolves as if there was no reaction. It is hence possible to estimate y_{ig} and τ_{ig} by reducing υ in Eq. 33 by the diffusion solution υ_0 in the Lagrangian frame

$$\frac{\partial \upsilon_0}{\partial \tau} = \frac{\partial^2 \upsilon_0}{\partial y^2} \tag{35}$$

$$\upsilon_0(-\infty) = 0 \tag{36}$$

$$\upsilon_0(+\infty) = -\eta \tag{37}$$

which yields the familiar solution:

$$\upsilon_0(\xi) = -\frac{\eta}{2}[1 + \operatorname{erf}(\xi)] \tag{38}$$

where $\xi = y/2\sqrt{\tau}$ and $\operatorname{erf}(\xi) = 2/\sqrt{\pi}\int_0^{\xi} e^{-\chi^2} d\chi$. This diffused profile caused by Taylor-Aris dispersion has an appreciable gradient only within the thermal boundary layer of thickness $2\sqrt{\tau}$. Temperature υ within the thermal boundary layer has been reduced to values significantly below zero by dispersion such that ignition can never take place within it. Consequently, $|y_{\text{ig}}| \gg 2\sqrt{\tau} \sim O(\chi^{-1/2})$ and we can expand Eq. 38 at larger y or ξ. [We shall demonstrate that $y_{\text{ig}} \sim O(\chi^{-1/2}|\ln \chi|^{1/2}) \gg O(\chi^{-1/2})$.] This can be done most conveniently by reducing υ of Eq. 33 with respect to υ_0, $\upsilon_1 = \upsilon - \upsilon_0$. Since ignition will take place in the heated region behind the thermal boundary layer when υ_1 is increased from zero to an order unity quantity, the spatial thermal gradient $\partial^2 \upsilon_1/\partial y^2$ is of order $\chi|\ln \chi|^{-1}$, which is smaller than the reaction term of order χ. This is in contrast to the thermal diffusion boundary layer region where $\partial^2 \upsilon_0/\partial y^2$ is of order $\eta\chi$, much larger than the reaction term of order $\chi e^{-\eta}$. We hence omit dispersion in the reduced equation to obtain:

$$\frac{d\upsilon_1}{d\tau} = \chi e^{\upsilon_0 + \upsilon_1} \tag{39}$$

which shows how the monolith just outside the boundary layer ignites from the diffused profile of Eq. 38. In essence, it is a competition between ignition and the encroaching boundary layer. We follow the temperature evolution of a point $y < 0$ behind the shock at $y = 0$. This point entered the monolith at $\tau = -y$ and we shall estimate the time it ignites by integrating Eq. 39

$$\int_0^{\infty} \frac{d\upsilon_1}{e^{\upsilon_1}} = 1 = \chi \int_{-y}^{\tau_{\text{ig}}} e^{\upsilon_0(\xi)} d\tau \tag{40}$$

which defines $\tau_{\text{ig}}(y)$ implicitly. Note that, strictly speaking, υ_1 cannot go to infinity since it would then induce an infinite spatial gradient at y and hence violate our assumptions of negligible gradient for υ_1 in Eq. 39. However, as was in the case of Eq. 11 and Figure 2, the exponential in the integrand on the left of Eq. 40 allows us to replace the order unity ignition temperature by infinity without significant error.

Expanding Eq. 38 for large ξ, we get

$$\upsilon_0(\xi) \sim \frac{2\eta}{\xi\sqrt{\pi}} e^{-\xi^2/4}\left[1 - \frac{2}{\xi^2} + \frac{12}{\xi^4} - \frac{120}{\xi^6} + \ldots\right] \tag{41}$$

whose oscillating signs yield a very slowly converging series. Nevertheless, we retain only the leading-order term for simplicity and, approximating e^{υ_0} in Eq. 40 by $1 + \upsilon_0$ obtain

$$\tau_{\text{ig}} \sim \chi^{-1} - y + \frac{4\eta y^2}{\sqrt{\pi}} \int_{y/\sqrt{-y}}^{y/\sqrt{\tau_{\text{ig}}}} \frac{e^{-\xi^2/4}}{\xi^4} d\xi \tag{42}$$

Since $-y \sim O(\chi^{-1/2}|\ln \chi|^{1/2})$ from earlier estimates while $\tau_{\text{ig}} \sim O(\chi^{-1})$, we can replace the lower limit of the above integral by $-\infty$. In the limit of $y/\sqrt{\tau_{\text{ig}}}$ approaching infinity, the integral can be estimated to yield, as χ approaches zero

$$\tau_{\text{ig}}(y) \sim \chi^{-1} - y - \frac{8\eta y^2}{\sqrt{\pi}} \left(\frac{y}{\sqrt{\tau_{\text{ig}}}}\right)^{-5} e^{-y^2/4\tau_{\text{ig}}} \tag{43}$$

which yields the ignition temperature as a function of y, the distance behind the front. Ignition takes place at y_{ig} where $\tau_{\text{ig}}(y)$ exhibits a minimum. An estimate of y_{ig} can be obtained by taking the derivative of Eq. 43 to obtain:

$$y_{\text{ig}} \sim -2\chi^{-1/2}|\ln(\chi^{1/2}/\eta) + c|^{1/2} \tag{44}$$

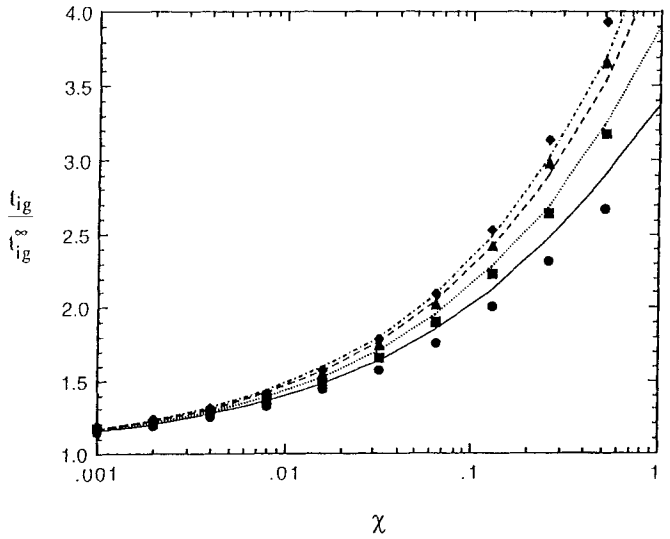

Figure 4. Ignition time from numerical integration of Eqs. 5 and 6 vs. small-χ analytical prediction of Eq. 45.

The η values are 2 (●), 4 (■), 8 (▲), 12 (◆), and the curves are the analytical results.

where c is estimated to be $-\ln 2$ numerically. Hence, at small χ, $|y_{ig}|$ is of order $\chi^{-1/2}|\ln \chi|^{1/2}$ which is larger than the $O(\chi^{-1/2})$ width of the thermal boundary layer as we claimed earlier. Substituting Eq. 44 into Eq. 43, we obtain a leading order estimate of the ignition time at small χ:

$$(\tau_{ig}/\tau_{ig}^{\infty}) = (t_{ig}/t_{ig}^{\infty}) = \tau_{ig}\chi = 1 + 2\sqrt{\chi}\left|\ln\left(\sqrt{\chi}/2\eta\right)\right|^{1/2} \quad (45)$$

The awkward χ dependence is a result of expanding the erf function of the diffusion profile v_0. It is clear that at small χ, ignition takes place a small distance y_{ig} just behind the thin thermal boundary layer at the front. We hence refer to this small χ ignition as downstream ignition since it occurs near the shock front which has propagated significantly downstream from the inlet. Remarkably, estimate (Eq. 45) is found to be accurate to within 5% of the simulated result from Eqs. 17 and 18 for $\chi < 0.3$ for all η larger than 2.0 as can be seen in Figure 4.

Fast Reaction Limit ($\chi \sim 1$)

As χ increases, Eq. 44 suggests that the ignition point moves far upstream such that it actually takes place at the leading edge of the monolith. This occurs when the reaction rate is fast such that χ is large and the reaction has progressed significantly before the Taylor-Aris dispersion has developed. The latter requires time θ of $O(1)$ as is evident from the eigenvalue -1 of Eq. 27 at large γ. In this limit, the large-time asymptotic behavior (Eq. 28) becomes invalid and ignition has already taken place before Eq. 32 becomes valid because of the poor interphase communication. We are hence interested in the dynamics before the solid and gas temperatures equilibrate. At this large-χ limit of weak interphase interaction, the gas temperature cools off only slightly downstream before the ignition occurs. The solid temperature does not follow the gas temperature adiabatically as in Eq. 30 of

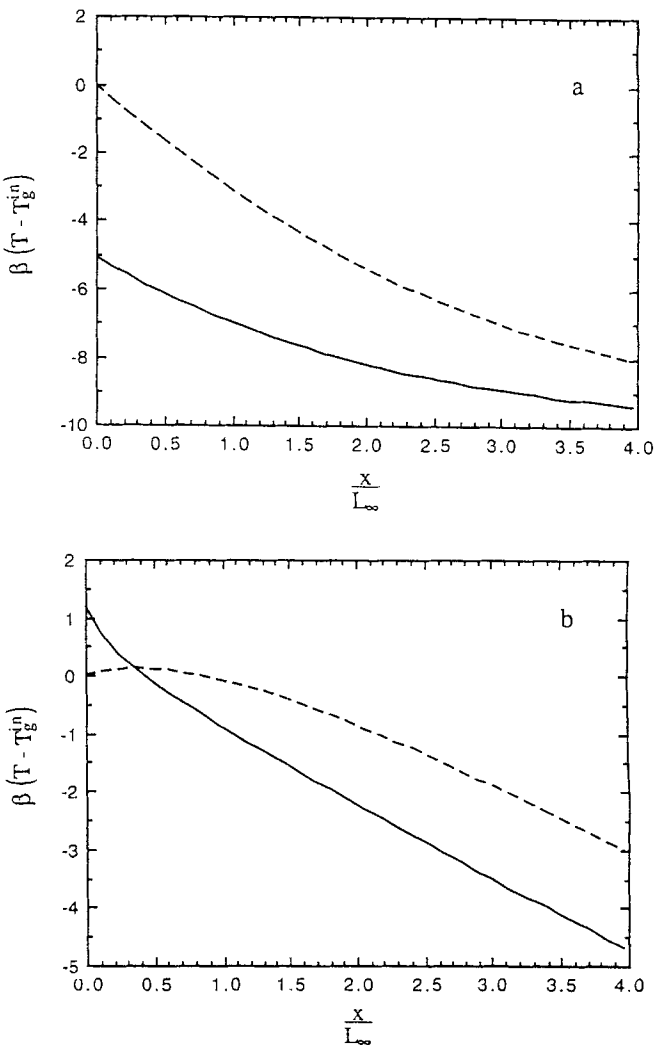

Figure 5. Large-χ solid (——) and gas (----) temperature evolution for $\chi = 1.45$ and $\eta = 10.12$ at $(t/t_{ig}^{\infty}) = 1.0$ in 5a and 5.0 in 5b.

The ignition occurs at $(t/t_{ig}^{\infty}) = 5.4$.

the small-χ mechanism. Due to the small interphase interaction and the slow decay of the gas temperature downstream, the leading-edge solid temperature is heated more than any point downstream and ignition occurs at the leading edge of the monolith. As the solid temperature rises prior to ignition, it can exceed the gas temperature at the leading edge as shown in Figure 5. This further affects the ignition time and its estimate must be carried out with a different asymptotic analysis.

At this large χ limit of fast reaction, the dynamics is dominated by the reaction term and the characteristic time should be t_{ig}^{∞} and the characteristic length for the gas phase $t_{ig}^{\infty}U_{eff} = L_\infty$. In terms of Eq. 18, a balance of the time evolution term with the reaction term that drives it shows that $\tau \sim \chi^{-1}$ which is equivalent to $t \sim t_{ig}^{\infty}$. We hence define a new dimensionless time $\bar{t} = \tau\chi = \theta\chi/\gamma$ where θ is the dimensionless time for the small-χ limit in Eqs. 23 and 24. The characteristic length L_∞ was used in the definition of the dimensionless coordinate z in the same equations and we retain it here. It corresponds

to a much shorter physical length here. Hence, in the large-χ limit, the appropriate equations are

$$\frac{1}{\gamma}\frac{\partial u}{\partial \tilde{t}} = \chi^{-1}(v-u) - \frac{\partial u}{\partial z}$$

$$\frac{\partial v}{\partial \tilde{t}} = \chi^{-1}(u-v) + e^{v}$$

The first equation shows that, to leading order for γ large, $\partial u/\partial z$ vanishes within the leading-edge boundary layer of width L_∞. Hence, $u = 0$ due to the boundary condition (Eq. 19). The poor interphase communication has not removed much of the gas thermal energy within this leading edge boundary layer. Consequently, the front-edge solid temperature can be described by Eq. 18 in the original variables

$$\frac{\partial v}{\partial \tau} = \chi e^{v} - v \quad v(0) = -\eta \tag{46}$$

and a slow heating of the leading edge takes place until ignition occurs. Note that unlike the small-χ slow reaction limit, there is no equilibration between the temperature of the two phases and an effective equation cannot be written. However, the large capacitance ratio γ allows us to ignore the dynamics of the gas phase and the short L_∞ allows us to neglect any gas-phase gradient. As a result, only homogeneous solid thermal dynamics need to be considered and explicit dependence on γ again disappears in this large-χ limit, although the remaining two parameters χ and η depend on γ implicitly. It is a simple matter to estimate the ignition time by integrating Eq. 46 to yield

$$\tau_{ig}\chi = \frac{\tau_{ig}}{\tau_{ig}^{\infty}} = \frac{t_{ig}}{t_{ig}^{\infty}} = \int_{-\eta}^{\infty} \frac{dv}{e^{v} - v/\chi} \tag{47}$$

This integral becomes singular for χ less than

$$\chi_c = e^{-1} \tag{48}$$

This is a good demarcation point for the validity of the present large χ analysis. For $\chi \to \infty$, Eq. 47 indicates that τ_{ig} is of order χ^{-1} as is consistent with our scaling, or equivalently, t_{ig}/t_{ig}^{∞} approaches a constant e^{η} which is dependent on the preheating η. Hence, unlike the small χ asymptote, the large χ asymptote for (t_{ig}/t_{ig}^{∞}) is sensitive to preheating. The function (t_{ig}/t_{ig}^{∞}) hence blows up at $\chi = e^{-1}$, decays very rapidly to a minimum at a slightly larger χ, and approaches the asymptote e^{η} very slowly as shown in Figure 6. Most realistic large χ monoliths, however, operate in the slowly varying region between the minimum and the e^{η} asymptote where $\chi \sim O(1)$. We can obtain an accurate analytical estimate for this region even though our equation is strictly valid only for large χ. This is possible when η is large. Expanding Eq. 47 in η, one obtains

$$\frac{d}{d\eta}\left(\frac{t_{ig}}{t_{ig}^{\infty}}\right) = \frac{1}{e^{-\eta} + \eta/\chi} \sim \frac{\chi}{\eta} \quad \text{for} \quad 1 \ll \chi \ll \eta e^{\eta} \tag{49}$$

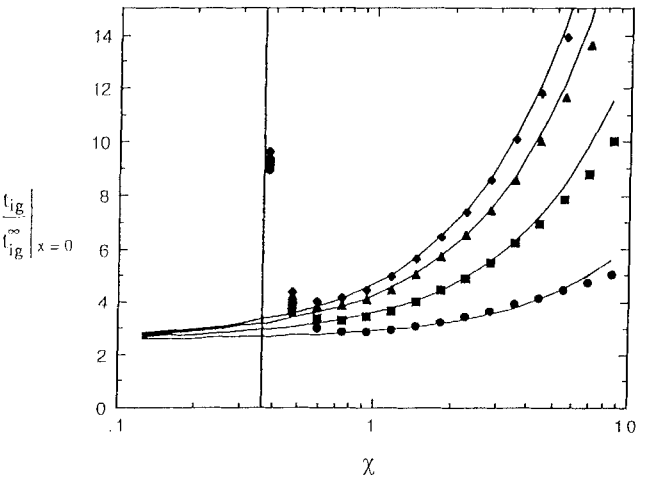

Figure 6. Comparison of computed ignition time at the leading edge $\eta = 2$ (●), 4 (■), 8 (▲), 12 (◆) to the analytical prediction of Eq. 51 in solid curve.

Note that the leading edge never ignites for $\chi < \chi_c = e^{-1}$.

Integrating once, one obtains

$$(t_{ig}/t_{ig}^{\infty}) \sim \chi \ln \eta + f(\chi) \tag{50}$$

provided χ is not too large. We find numerically that $f(\chi)$ is a linear function of χ in the intermediate region between the minimum near e^{-1} and the constant at e^{η}. This is evident in Figure 6. Numerically expanding $f(\chi)$ near $\chi = 1.0$, one obtains

$$(t_{ig}/t_{ig}^{\infty}) \equiv 2.50 + (\ln \eta - 0.344)\chi \tag{51}$$

which is within 5% of Eq. 47 for the large region of $1.0 < \chi < 4.0$ and $2.0 < \eta < 10.0$ where most large-χ (heated) monoliths operate.

For $\eta \ll 1$, (t_{ig}/t_{ig}^{∞}) does not approach a minimum and it can be estimated with a large χ expansion of Eq. 47 to yield

$$(t_{ig}/t_{ig}^{\infty}) = e^{\eta}\left[1 - \frac{e^{\eta}}{4\chi}(2\eta - 1)\right] \tag{52}$$

This is accurate within 10% for $\eta < 1.0$ and $1.0 < \chi < 4.0$.

The accuracy of Eqs. 45 and 51 for the case of $\eta = 7.59$, corresponding to the standard condition, is demonstrated in Figure 7 over three decades of χ! The numerical result is obtained by integrating Eqs. 16 and 17 with an implicit finite-difference scheme. The demarcation between downstream ignition and leading-edge ignition is represented by the discontinuity of the slope of t_{ig}/t_{ig}^{∞} at $\chi \sim 0.4$, close to $\chi_c = e^{-1}$ of Eq. 48. The transition from the downstream low-χ mechanism to the leading edge large-χ mechanism as χ increases through e^{-1} is also evident in Figure 8 which depicts the ignition location L_{ig} as a function of χ. A rapid decay to very small values of L_{ig} occurs at $\chi \sim 0.5$, close to the transition value of e^{-1}. We shall use these accurate estimates of t_{ig}

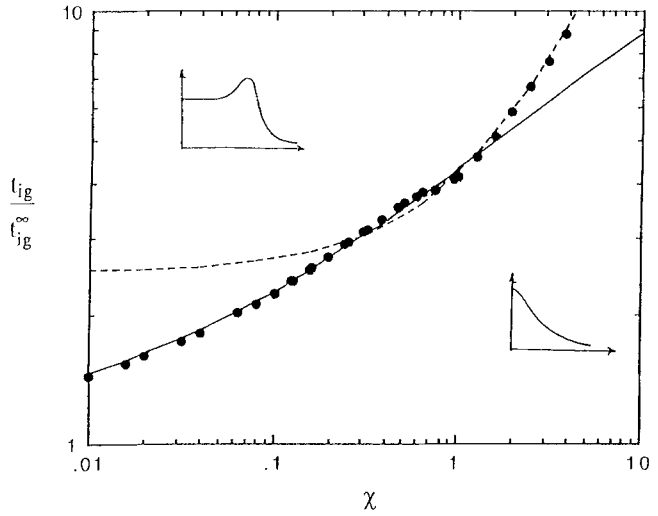

Figure 7. Ignition time as a function of χ for the standard value of $\eta = 7.59$.

Numerical computation (●), analytical prediction of Eq. 45 (——), that of Eq. 51 (– – – –). The demarcation between the small-χ and large-χ mechanisms are at $\chi_c \sim e^{-1}$. An inflection point appears in the computed value at this point.

to design a fast igniting catalytic converter in the next section. We first note, however, that the analysis in this section is carried out at the leading edge because that is where the ignition takes place before the Taylor-Aris dispersion develops in the channels. After the ignition, when the heat-releasing reactants have been depleted, the heating of the entire monolith by the thermal front (established at the leading edge by the ignition) is still affected by Taylor-Aris dispersion. In essence, Eqs. 31 or 32 without the reaction term governs the front propagation long after the ignition and downstream from the leading edge. The effective dispersion of this front propagation phenomenon is still given by Eq. 14 and the front speed by U_{eff} of Eq. 10.

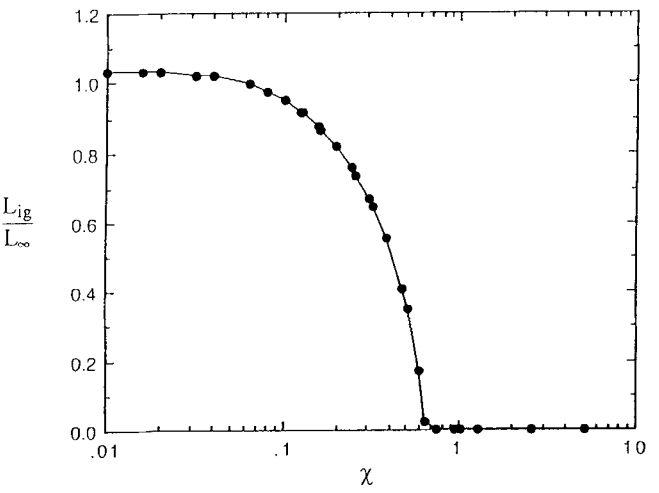

Figure 8. Computed ignition point as a function of χ for the standard value of $\eta = 7.59$.

The transition to leading-edge large-χ mechanism occurs at about $\chi_c \sim e^{-1}$.

Table 2. Comparison to Oh and Cavendish's Simulations

Dependence of Parameters on T_g^{in} and n

$$\Delta T = T_g^{\text{in}} - (T_g^{\text{in}})_0 \quad \epsilon = [1 - 2\Delta z\sqrt{n}\,]^2$$

$$\eta = \eta_0 + \beta\Delta T$$

$$\chi = \chi_0 e^{\beta\Delta T}(n_0/n)((T_g^{\text{in}})_0/T_g^{\text{in}})^{0.832}$$

$$t_{ig}^{\infty} = (t_{ig}^{\infty})_0 e^{-\beta\Delta T}(1-\epsilon)/(1-\epsilon_0)$$

$T_g^{\text{in}} = 600$ K	Oh and Cavendish		Eq. 45		$\eta = 7.59$	
n	t_{ig}	t_{ig}/t_{ig}^{∞}	t_{ig}	t_{ig}/t_{ig}^{∞}	t_{ig}^{∞}	χ
31 cells/cm^2	42 s	2.96	38 s	2.65	14.2 s	0.197
46.5 std.	46	2.69	41	2.40	17.1	0.131
93	56	2.40	47.4	2.04	23.3	0.066

$T_g^{\text{in}} = 700$ K	Oh and Cavendish		Eq. 51		$\eta = 10.12$	
n	t_{ig}	t_{ig}/t_{ig}^{∞}	t_{ig}	t_{ig}/t_{ig}^{∞}	t_{ig}^{∞}	χ
31 cells/cm^2	10.0 s	8.8	7.7 s	6.8	1.13 s	2.18
46.5 std.	9.8	7.2	7.3	5.4	1.36	1.45
93	9.5	5.1	7.3	7.3	1.86	0.73

Optimal Design of a Catalytic Converter System

In the previous two sections, we have compared our analytical theories to the model Eqs. 5 and 6 or their dimensionless version Eqs. 17 and 18. However, Eqs. 5 and 6 have been derived with two major approximations, the omission of reactant consumption and the zeroth-order kinetic approximation of Eq. 4 and Figure 1. A more stringent comparison would be to test them against the full model of Oh and Cavendish. This quantitative comparison is also instructive because many of their observations can be faithfully interpreted by the current theory.

Using their standard conditions listed in Table 1 here, which corresponds to a standard catalytic converter in the benchmark step-change cold start test, we obtain the values $\chi = 0.13$ and $L_{\infty} = 14.7$ cm and, from Figure 8, $L_{ig} = 13.2$ cm. This indicates that the standard monolith in the base case ignites by the small-χ mechanism downstream. In fact, from our theory, the earliest ignition would occur just beyond the end of the 10 cm long monolith! In reality, of course, the ignition will take place exactly at the end of the monolith and our prediction of t_{ig} should be lower than that resulting from the simulations of Oh and Cavendish since $L < L_{ig}$. Ignition at the monolith exit for the standard condition is clearly observed in the simulation result in Figure 1 of Oh and Cavendish (1982) and their simulated ignition time of 46 s is about 10% higher than our predicted value of 41 s from Eq. 45 (Table 2). We have identified the ignition point in their simulations as where the plot of CO conversion vs. time reaches an inflection point. In Oh and Cavendish's simulation, this downstream ignition is followed by a slow creep of the thermal front towards the front. This front propagation is mostly through thermal conduction in the solid. From the classical theories of flame propagation (Zeldovich et al., 1985) and the most recent study of front propagation in a catalytic converter by Please et al. (1994), thermal front propagation scales as $\sqrt{\alpha_s}$ if all other conditions are the same. As mentioned earlier, the apparent thermal diffusion in Eq. 14, due to the Taylor-Aris mechanism, is strictly a downstream mechanism and it does not accelerate upstream front propagation. This front propagation phenomenon is beyond our ignition

theory due to the omission of reactant consumption. However, for the standard conditions, Oh and Cavendish observed that 250 s is required after ignition for the thermal front to propagate over the entire monolith and hence ignite the entire converter.

A much different behavior is encountered if the converter ignites by the large-χ mechanism. In this case ignition occurs at the leading edge and, due to their relatively high reaction rates at elevated temperatures, CO and H_2 are entirely consumed in the first few centimeters of the monolith. Since these gases provide the only significant source of heat, the heating of the rest of the converter essentially corresponds to a thermal front propagation problem without reaction, in which the gases entering the remainder of the converter are at the adiabatic reaction temperature of 900 K. (Without reaction, the χ term vanishes in Eqs. 26 and 27 even if the ignition took place by the large-χ mechanism at the leading edge. In other words, Eqs. 29 or 32 without the reaction term remain valid away from the leading edge if there is no reaction.) This front will propagate with a speed U_{eff}; thus, the time to heat the rest of the monolith will be on the order of L/U_{eff} which, for the standard conditions listed in Table 1, is approximately 12 s. Taylor-Aris dispersion will increase this slightly due to a smearing out of the thermal front, but the entire monolith should be at reaction temperature approximately 15 s after leading edge ignition. Although CO and H_2, the two fastest reactions, are almost completely consumed soon after light off within a small area of the monolith at $t = t_{\text{ig}}$, the conversion of C_3H_6 and most appreciably, CH_4 and NO, require the ignition of the entire monolith. This is why monoliths are typically designed to be 10 cm or more in length. Consequently, although our theory predicts a longer t_{ig} for the large-χ mechanism if t_{ig}^{∞} is held constant (Figure 7, for example), it is far more efficient to ignite the converter at the leading edge with the large-χ mechanism. The standard catalytic converter in the benchmark test is hence poorly designed in the sense that the ignition location is behind the monolith and the small-χ mechanism requires a long front propagation time of 250 s. This is the key reason why it has such a poor startup performance.

Nevertheless, much of the effects of the new conditions Oh and Cavendish imposed on the standard converter can now be understood. For example, the ignition length of a converter with infinitely fast interphase communication L_{∞} can be written as

$$L_{\infty} = \frac{W_g (c_p)_g}{A\beta} \tag{53}$$

where $W_g = \rho_g U \epsilon$ is the superficial gas mass velocity. The key parameter χ, on the other hand, can be written as in Eq. 16.

$$\chi = \frac{\alpha_{\text{eff}}}{U_{\text{eff}}^2 t_{\text{ig}}^{\infty}} \sim \frac{11}{48} \frac{A\beta a^2}{\alpha_g \epsilon (\rho c_p)_g} \tag{54}$$

which is independent of the gas flow. This is an important result due to the fact Taylor-Aris dispersion α_{eff} scales as the velocity squared. It implies that we can alter the gas velocity without changing the value of χ or the ignition time—an important freedom in the design of a fast-igniting converter that minimizes the length of a converter. Hence, from Eq. 53, the ignition location scales as W_g and for the standard condition, $L_{\text{ig}} = 13.2$ cm. Any increase in the mass-flow rate will place the ignition point so far outside the monolith that ignition will never occur. This is clearly seen in Oh and Cavendish's simulation when the mass-flow rate is increased from 40 g/s to 60 g/s. This is another danger of small-χ ignition with L_{∞} very close to the actual monolith length L. Slight increases in the gas flow or decreases in the feed temperature will significantly lengthen the ignition time!

The most conclusive comparison to Oh and Cavendish's simulation are the opposite effects of cell density n at the standard feed temperature of $T_g^{\text{in}} = 600$ K and the preheated condition of $T_g^{\text{in}} = 700$ K. They varied the cell density while holding the wall thickness $2\Delta z$ of the square channels constant, and hence the void fraction varies with n according to

$$\epsilon = [1 - 2\Delta z \sqrt{n}\,]^2 \tag{55}$$

Since $a^2 = \epsilon/4n$ for square channels, the dependence of χ on n with Δz constant can be derived from Eq. 54:

$$\chi = \frac{11}{192} \frac{A\beta}{n k_g} \tag{56}$$

where k_g is the gas conductivity. Hence, increasing n with Δz constant decreases χ and ϵ, but increases t_{ig}^{∞}. In essence, increasing the cell density increases the solid heat capacity $(1-\epsilon)(\rho c_p)_s$ and hence increases the homogeneous ignition time t_{ig}^{∞} because it requires more heat to raise the solid temperature. On the other hand, it also decreases the channel radius a and hence increases interphase communication or, equivalently, decreases Taylor-Aris dispersion α_{eff} of Eq. 14. From Eq. 45, it is clear that for the small-χ mechanism where the effect of χ on t_{ig} is minimal, the effect on t_{ig}^{∞} dominates and the actual ignition time should increase with n. This is exactly what was observed by Oh and Cavendish (1982). More impressively, our prediction of t_{ig} and $(t_{\text{ig}}/t_{\text{ig}}^{\infty})$ from Eq. 45 is within 15% of his computed values as shown in Table 2! The simple design Eq. 45 is accurate even when n is varied by as much as 100% from the standard. This suggests the omission of reactant consumption and the zero-order kinetics approximation are good assumptions for the ignition phenomenon.

A more stringent comparison is against their simulations for the converter when preheating is used to raise T_g^{in} to 700 K. From Figure 1, it is clear that our zeroth-order kinetics is expanded about the standard condition of 600 K and it overpredicts the reaction rate by as much as 20% near 700 K. One hence expects a comparable under prediction of t_{ig}. Preheating affects t_{ig}^{∞}, η and χ. Some simple algebra shows that a ΔT increase in the T_g^{in} from the standard 600 K increases χ, but decreases t_{ig}^{∞} by the same factor of $e^{\Delta T\beta}$ and increases η by $\beta\Delta T$ as shown in Table 2. There is an additional influence on χ due to the temperature dependence of the gas conductivity k_g. Consequently for a preheating of $\Delta T = 100$ K, χ increases from 0.13 of the standard condition to 1.45. As a result, a preheated converter with $\Delta T = 100$ K ignites by the completely different large-χ mechanism at the leading

edge. The ignition time is now governed by Eq. 51. Since t_{ig}^{∞} scales as $\sqrt{n}$ while χ scales as n^{-1}, Eq. 51 indicates that the effect of n at $T_g^{in} = 700$ K depends on the magnitude of the two terms on the right of Eq. 51 for the preheated reference condition of $n = 46.5$ and $\eta = 10.12$ (Table 2). Since the second term (3.81) is larger than the first (2.50), the χ term dominates and increasing n should decrease χ and also t_{ig}, opposite of the standard case of $T_g^{in} = 600$ K. This opposite trend of increasing n is confirmed by Oh and Cavendish's simulation results reproduced in Table 2. In fact, a simple calculation yields that this reversal of the effect of increasing n begins at $\beta\Delta T = 2.27$ or a preheating of 90 K. Below $T_g^{in} =$ 690 K, increasing n increases the ignition time t_{ig} while above 690 K, it decreases the ignition time. The latter occurs because at the large-χ limit, the effect of n on interphase transport through the pore radius as measured by χ is more pronounced than the effect on the homogeneous reaction time through the solid heat capacity. Quantitatively, Eq. 51 also yields predictions of t_{ig} that are no more than 30% below Oh and Cavendish's simulation result. This is quite satisfactory because the reaction rate is known to be overpredicted by 20% near 700 K. In fact, if we refit the kinetics by expanding about 700 K instead of 600 K to obtain $\beta = 0.0209$ and $A = 2.10$ J/s·cm^3, η now becomes 8.36 and $t_{ig}^{\infty} = (1.60, 1.90, 2.63$ s) and $\chi = (1.54, 1.02, 0.51)$, respectively, for $n = 31$, 46.5 and 93 cells/cm^2 at $T_g^{in} = 700$ K. Using these values and Eq. 51, we obtain $t_{ig} = (8.4, 8.3, 9.0$ s) or $(t_{ig}/t_{ig}^{\infty}) = (5.25, 4.37, 3.42)$ which are within 20% of Oh and Cavendish's simulation results in Table 2. The remaining discrepancy is likely due to neglecting mass-transfer resistance when calculating the reaction rate. This is much more significant for the preheated case, as the overall reaction rate is much higher under these conditions.

We now consider alternatives other than preheating to accelerate the ignition process. From our arguments on thermal front propagation, it is clear we want the catalytic converter to ignite at the leading edge by the large χ mechanism. Consequently, χ needs to be raised from its standard value of 0.13 to above 0.5. However, increasing χ increases (t_{ig}/t_{ig}^{∞}) as shown in Figure 7 and one must also reduce t_{ig}^{∞} to make t_{ig} smaller than the current 46 s. There are several possible ways to achieve this other than preheating. One is to increase the void fraction since t_{ig}^{∞} scales as $(1-\epsilon)$ as seen in Eq. 12 while χ scales as ϵ^{-1} as in Eq. 54. However, even with the most porous metal converter supports that have been suggested, ϵ cannot be increased significantly beyond the current 0.68. Another is to increase catalyst loading, viz. increase A, since χ scales as A while t_{ig}^{∞} scales as A^{-1}. However to reach $\chi =$ 0.5, one would need four times the current catalyst loading while t_{ig}, now calculated by Eq. 51 using a t_{ig}^{∞} that is four times smaller, is still at a relatively large value of 15 s. Using metal converters to lower the solid heat capacity is also not promising. They do not provide a lower $(\rho c_p)_s$ and the solid fraction $(1-\epsilon)$ can only be reduced by at most a factor of 3 for similar cell densities unless very thin and structurally unstable foils are used. This is not quite sufficient to raise χ to above χ_c. Another poor idea is to increase the solid thermal diffusivity α_s with a metal substrate. The highest realistic α_s is for a stainless steel substrate with $\alpha_s = 0.6$ cm^2/s. This is still significantly lower than α_{eff} of the Taylor-Aris mechanism and hence does not contribute to the ignition process as Oh and Cavendish have observed from their simulation. An increased α_s will accelerate the upstream front propagation of the small-χ mechanism by a factor of $\sqrt{\alpha_s}$. However, purely convective downstream thermal front propagation of the large-χ mechanism remains much faster. It should also be clear from Table 2 that reducing n within the realistic limits cannot increase χ significantly. We hence conclude that the most expedient way of increasing χ to beyond χ_c to achieve leading-edge ignition and also decreasing t_{ig}^{∞} is to preheat the current converter. A preheat of $\Delta T = 100$ K will reduce t_{ig} from 46 s to 9.8 s while the front propagation time will be reduced from 250 s to 15 s. It is actually unnecessary to change the current converter if preheating of 100 K is achievable and the above ignition times are acceptable.

Preheating by an electric heater remains unattractive, however, because of the required battery. Hence we use our theory to design an igniter to preheat the current converter without any electric heating. In the design of the igniter, our sole purpose is to increase the T_g^{in} to the current converter by preheating. It is unnecessary to ignite the entire monolith of the igniter since the igniter is not intended as a catalytic converter. As such, we are not concerned about the thermal front propagation factor and design our igniter for the faster small-χ ignition mechanism. Consequently, many improvement options that proved unsuitable for the converter because they decrease χ as well as t_{ig}^{∞} are actually viable for the igniter. We begin by using a commercial Celcor monolith (Gulati et al., 1990) with the lowest solid heat capacity $(1-\epsilon)(\rho c_p)_s$ which is a factor of 2.35 below the standard value. It has a cell density $n = 62$ cells/cm^2, higher than the standard 46.5. If we now introduce a catalyst loading three times the standard value on this monolith, we lower t_{ig}^{∞} by a factor of 2.35×3 or $t_{ig}^{\infty} = 2.42$ s. The χ value, on the other hand, is increased by a factor of 3(46.5/62) to 0.293. This is still below χ_c and Eq. 45 yields a prediction of $(t_{ig}/t_{ig}^{\infty}) = 2.98$ or $t_{ig} = 7.2$ s. More porous metal monoliths or higher cell densities can reduce the t_{ig} of this igniter to even lower values.

It is highly undesirable to use an entire monolith with three times the catalyst loading of the standard converter as an igniter due to high catalyst costs. Fortunately, the inlet gas temperature to the converter need only be raised to $T_g^{in} = 700$ K while the gas temperature leaving the igniter is at the adiabatic temperature of 900 K. Consequently, 2/3 of the exhaust can be safely bypassed around the igniter. This bypass does not affect the values of η, χ and t_{ig}^{∞} estimated above as is evident from Eqs. 12, 21 and 54 since all of them are independent of the gas velocity—the ignition time t_{ig} is hence unaffected. However, from Eq. 53 it reduces by a factor of 3 the L_{∞} that has already been reduced by a factor of 3 from the standard due to the increased loading. This yields an L_{∞} of $(14.7/9) = 1.6$ cm. From Figure 8, L_{ig} for the given χ value of 0.293 is then 1.1 cm. If we assign an igniter length of 2 cm to allow for a possible two-fold increase in the standard mass-flow rate which can result, for example, from an extremely fast acceleration from cold start (a typical heavy load is only $W = 64$ g/s) the igniter is still only 1/5 of the length of the converter. Hence, even with 3 times the catalyst loading, the amount of catalyst in the igniter is only 60% of the total in the converter. Obviously, if modern metal monoliths with low solid heat capacities and high void fraction can be safely used as the igniter, the loading can be reduced even further.

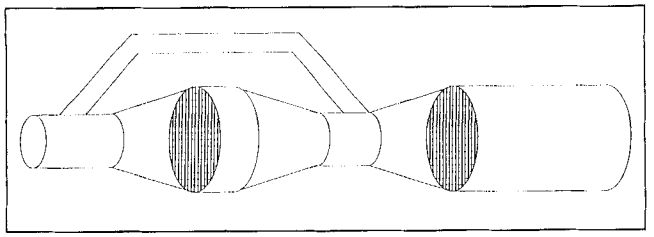

Figure 9. Fast-igniting converter system with an igniter upstream of a standard ceramic monolith.

The bypass is designed to allow for 2/3 of the exhaust. The igniter is shorter than the standard monolith but with a higher catalyst loading per unit volume. The igniter can be switched off after light off by bypassing all the exhaust.

Heat loss from the gas between the igniter and the converter is negligible due to the large gas velocity U. This offers the attractive installation advantage of leaving the current converter intact and simply placing the igniter in the exhaust pipe upstream, as shown in Figure 9 where the bypass is designed to allow 2/3 of the exhaust to bypass the igniter. The additional pressure drop introduced by the igniter is also only about 10% of the converter itself, and hence is negligible.

With the above igniter design, the igniter lights off in about 7 s and T_g^{in} to the converter is raised to 700 K at that moment. (The adiabatic temperature rise is 300 K but, due to the 2/3 bypass, the gas temperature reaching the converter is at 700 K.) During that 7 s, however, the leading edge of the catalytic converter has already been raised from 300 K to 500 K. (The cold igniter also cools the exhaust from 600 to 500 K before it ignites.) Since ignition at $T_g^{\text{in}} = 700$ K takes place by the large-χ mechanism at the leading edge, the ignition actually takes place from 500 K and not 300 K. As a result, ignition time of the converter after the igniter has lighted off is significantly lower than the 9.8 s in Table 2. If we use 500 K as T_s^0, η is now reduced to $0.0253(700-500) = 5.06$ instead of the 10.12 in Table 2. The values of χ and t_{ig}^{∞} for the converter are independent of T_s^0 and remain at the values of 1.45 and 1.36 s at $T_g^{\text{in}} = 700$ K. Figure 6 shows that, at these η and χ values, Eq. 51 is still an accurate estimate of t_{ig} and we obtain a converter ignition time of 5.9 s. This is verified in Figure 10 where simulation of Eqs. 5 and 6 with $T_g^{\text{in}} = 500$ K for 7 s is increased to 700 K. Ignition occurs in about 6 s after the second increase in T_g^{in}. Note that the partial consumption of CO and H_2 by the igniter actually increases the reaction rate in the converter due to the poisoning effects of the CO. This effect has not been accounted for in the above simulation, and should reduce the ignition time by a further 10%.

It is then clear the igniter lights off in about 7 s in the above design and the downstream converter lights off in approximately 6 s after that. The total of 13 s is about 25% of the current ignition time of 46 s and hence should reduce the fast-burning CO and H_2 emissions by 75%. The other pollutants, NO and CH_4, require heating the entire catalytic monolith to reaction temperatures and hence must await the thermal front propagation. We also reduce this time from 250 s to about 15 s since the converter now ignites at the leading edge by the large-χ mechanism due to preheating by the igniter. There should hence be approximately a 90% reduction in these emissions as well. Additional improvements in this performance may be possible since the catalyst of the igniter

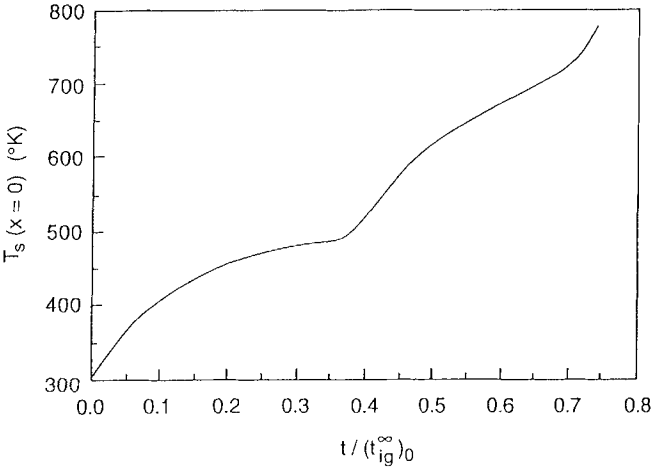

Figure 10. Solid temperature evolution at the leading edge of the converter in Figure 9.

The igniter upstream lights off in 7 s or 0.38 in the dimensionless time units. The converter has already been heated to 500 K at this point and it continues to be heated by the heated exhaust from the igniter such that ignition occurs at 13.0 s (0.76 dimensionless time). The conditions are $\chi_o = 0.13$, $T_s^o = 300$ K and $T_g^{\text{in}} = 500$ K for dimensionless time less than 0.38 and 700 K after that.

need only oxidize CO and H_2; reduction of NO is not required. The catalyst can therefore be simplified, which may improve reaction kinetics during the critical cold start period. Note that the igniter can also be switched out of the exhaust stream after ignition to improve the life of the catalyst in the igniter and possibly permit the use of lighter weight metal monoliths.

Summary and Discussion

We have used the zero-order kinetics approximation and asymptotic analysis to derive the analytical estimates of the ignition time in Eqs. 45, 51 and the less useful version of Eq. 52. They are shown to be quite accurate over the conditions of most step-response converters although the kinetic parameters A and β may need to be reevaluated to obtain a more accurate value of t_{ig}^{∞} for T_g^{in} significantly higher than the standard 600°K. The analysis also reveals the two distinct mechanisms for ignition, a fast downstream ignition at small χ with high interphase interaction and a slow leading-edge ignition at large χ with low interphase coupling. Thermal front propagation considerations stipulate that the converter should ignite by the large-χ mechanism and, to significantly reduce t_{ig}, preheating to $T_g^{\text{in}} = 700$ K is the only viable option. Instead of using an electric heater for preheating, we design an efficient igniter upstream of the current monolith that promises to light off the converter in 13 s. We design the igniter to ignite in the low-χ region and use our analysis to minimize the catalyst loading in the igniter such that only 60% of the catalyst in the converter is required in the igniter. The pressure drop introduced by the igniter is only about 10% of the standard converter itself, and hence is negligible.

With better monoliths and more efficient experimentation, we should be able to design an even better igniter. Detailed designs should include a three-dimensional model and radiative heat-transfer effects (Chen et al., 1988; Zygourakis, 1989;

gourakis, 1989; Lee and Aris, 1977). However, the two ignition mechanisms revealed in our study should still exist with the inclusion of these effects. Even the simple design equations offered by our asymptotic analysis of the pseudo-one-dimensional model are still quite accurate since flow maldistribution and radiation effects are not significant as far as ignition is concerned, although it may establish steep thermal fronts subsequently. For example, using conditions very similar to the standard case of Table 1 ($\epsilon = 0.64$ instead of 0.68 and $a = 0.05$ cm instead of 0.06 cm) but with $W = 25$ g/s instead of 40 and $T_g^{in} = 650$ K instead of 600, Chen et al. estimated in their Figure 12 that a 3-D monolith reactor with radiative heat transfer ignites at about 13 s. With twice the catalyst loading, their Figure 11 shows the converter lights off at 8.0 s and with one-third the loading, at about 28 s. All results are insensitive to whether the monolith is well insulated or whether flow maldistribution exists. The mass-flow W has no effect on t_{ig} since χ, η and t_{ig}^{∞} are all independent of W as seen in Eqs. 54, 21 and 12. The only significant change is the increase of T_g^{in} from 600 to 650 K which changes η to 8.86, χ to 0.327 and t_{ig}^{∞} to 3.45 according to the formulae in Table 2 with $\Delta T = 50$ K. Using Eq. 45, this yields $(t_{ig}/t_{ig}^{\infty}) = 3.12$ or $t_{ig} = 10.7$ s which is very close to Chen et al.'s 13 s. The doubling and trisecting of the catalyst loading changes χ proportionally to 0.653 and 0.11 and t_{ig}^{∞} to 1.72 and 10.35, respectively. Application of Eqs. 51 and 45, respectively, again yields $t_{ig} = 6.3$ s and 24 s which compare well with Chen et al.'s numerical values of 8.0 and 28 s. Modifications of β and A to more closely correspond to the kinetics in the vicinity of 650 K should further improve the agreement. The insensitivity of t_{ig} to W is also clearly shown in their Figure 14. It is impressive that our simple analytical formulae can predict the ignition time of a complex three-dimensional model with radiation to within 20%! The insensitivity to W is why flow maldistribution is unimportant as far as t_{ig} is concerned. The ignition location will, of course, be affected by the flow velocity in each pore channel. Radiative flow maldistribution and transverse dependence should, however, be more important in the propagation of the thermal front following ignition. The thermal front now needs to propagate in the radial direction and flow maldistribution and radiative heat transfer will also affect the speed of the thermal front. Nevertheless, the advantage of igniting near the entrance at large χ should still hold and our analytical theory should prove invaluable in the detailed design of a fast-igniting converter even if one deviates from the concept of an upstream igniter.

A particular concern for actual converter design is the constantly-varying conditions in a real startup that deviates from the current step-change standard test. Another is the poisoning of the highly loaded igniter. Once deactivated, the igniter actually acts as a heat sink and is extremely undesirable. Several possible solutions come to mind. Since the igniter only serves to extract heat from the exhaust and is not intended as a catalyst, a more stable catalyst can be used which only oxidizes CO or H_2, the main heat sources. Another attractive solution for both is the implementation of a controller that controls the by-pass such that large-χ ignition always occurs in the main converter even for highly transient startup conditions. The control loop can also bypass the igniter completely after the startup to minimize igniter poisoning. This control loop should be beneficial even if the preheating strategy is adopted. By preheating the igniter only, the heating requirement is minimized with a proper adjustment of the bypass at any given instant. With the availability of cheap and reliable controller chips and mass-flow meters, a "smart" exhaust system, not unlike the fuel control system, is definitely a possibility. An application of our understanding of the ignition process from the present theory to the design of a controller for commercial converters under realistic conditions will be reported in a future article.

Acknowledgment

The input of Se H. Oh was invaluable in our understanding of the ignition phenomenon. This research is partially funded by NSF under grants CTS-9112977 and CTS-9200210.

Notation

a = pore radius
A = preexponential factor of zeroth-order kinetics
c_p = heat capacity
C_g = gas-phase concentration
ΔH_i = heats of reaction
L_∞ = ignition point without dispersion
L_D = diffusion length of a boundary layer induced by Taylor-Aris dispersion
n = monolith cell density, cells/cm^2
R_i = reaction kinetics
t = time
t_{ig}^{∞} = ignition time of a homogeneous monolith
t_{ig} = ignition time
u = dimensionless gas temperature
U = linear gas velocity
U_{eff} = effective velocity of a solid thermal front
v = dimensionless solid temperature
W_g = superficial gas mass velocity
x = spatial coordinate
y = dimensionless spatial coordinate
z = scaled spatial coordinate
Δz = half-dimensional monolith wall thickness

Greek letters

α = thermal diffusivity
α_{eff} = effective thermal diffusivity of the solid phase due to Taylor-Aris dispersion
β = inverse Frank-Kamenetskii temperature
γ = heat capacity ratio
ϵ = void fraction
τ = dimensionless time
θ = scaled time
η = preheating
$\chi = (L_D/L_\infty)^2$ ratio of kinetics to interphase thermal interaction effects

Subscripts

eff = effective due to Taylor-Aris mechanism
ig = ignition
∞ = homogeneous or dispersionless
s = solid

Superscripts

0 = initial
° = reference point
in = inlet

Literature Cited

Amundson, N. R., and R. Aris, *Mathematical Methods in Chemical Engineering*, Vol. 2, Prentice-Hall, Englewood Cliffs, NJ (1973).

Aris, R., "On the Dispersion of a Solute by Diffusion, Convection and Exchange Between Phases," *Proc. R. Soc. London*, **A252**, 538 (1959).
Balakotaiah, V., and H.-C. Chang, "Dispersion of Chemical Solutes in Chromatographs and Reactors," *Phil. Trans. of Roy. Soc. London*, **A351**, 39 (1995).
Chen, D. K. S., E. J. Bissett, S. H. Oh, and D. L. V. Ostrom, "A Three-Dimensional Model for the Analysis of Transient Thermal and Conversion Characteristics of Monolithic Catalytic Converters," SAE paper 880282 (1988).
Eagle, A., and R. M. Ferguson, "On the Coefficient of Heat Transfer From the Internal Surface of Tube Walls," *Proc. Roy. Soc.*, **A127**, 540 (1930).
Flytzani-Stephanopoulos, M., G. E. Voecks, and T. Charng, "Modeling of Heat Transfer in Nonadiabatic Monolith Reactors and Experimental Comparisons of Metal Monoliths with Packed Beds," *Chem. Eng. Sci.*, **41**, 1203 (1986).
Gulati, S. T., K. P. Reddy, and D. F. Thompson, "High Temperature Strength Behavior of Ceramic Versus Metal Substrates," SAE paper 902170 (1990).
Heck, R. H., J. Wei, and J. R. Katzer, "Mathematical Modeling of Automotive Catalysts," *AIChE J.*, **22**, 477 (1976).
Kasoy, D. R., and A. Linan, "The Influence of Reactant Consumption on the Critical Conditions for Homogeneous Thermal Explosions," *J. Mech. Appl. Math.*, **31**, 99 (1978).
Lee, S. T., and R. Aris, "On the Effects of Radiative Heat Transfer Monoliths," *Chem. Eng. Sci.*, **32**, 827 (1977).
Leventon, W., "Pollution Fighters Target Auto Emissions," *Design News*, p. 129 (1993).
Oh, S. H., J. Bisset, and P. A. Battiston, "Mathematical Modeling of Electrically Heated Monolith Converters: Model Formulation, Numerical Methods, and Experimental Verification," *Ind. Eng. Chem. Res.*, **32**, 1560 (1993).
Oh, S. H., and J. C. Cavendish, "Design Aspects of Poison-Resistant Automobile Monolithic Catalytic Converter," *I&EC Prod. Res. Dev.*, **22**, 509 (1983).
Oh, S. H., and J. C. Cavendish, "Transients of Monolithic Catalytic Converters: Response to Step Changes in Feedstream Temperature as Related to Controlling Automobile Emission," *I&EC Prod. Res. Dev.*, **22**, 29 (1982).
Please, C. P., P. S. Hagan, and D. W. Schwendeman, "Light-off Behavior of Catalytic Converters," *SIAM J. Appl. Math.*, **54**, 72 (1994).
Roberts, A. J., "The Utility of an Invariant Manifold Description of the Evolution of a Dynamical System," *SIAM J. Math. Anal.*, **20**, 1447 (1989).
Taylor, G. I., "Dispersion of Soluble Matter in Solvent Flowing Slowly Through a Tube," *Proc. R. Soc. London*, **A219**, 186 (1953).
Wittenberger, W. A., and J. E. Kubsh, "Electrically Heated Metal Substrate Durability," SAE paper 910613 (1991).
Young, L. C., and B. A. Finlayson, "Mathematical Models of the Monolith Catalytic Converter: I," *AIChE J.*, **22**, 331 (1976).
Zeldovich, Ya. B., G. I. Barenblatt, V. B. Librovich, and G. M. Makhviladze, *The Mathematical Theory of Combustion and Explosions*, Consultants Bureau, New York (1985).
Zygourakis, K., "Transient Operation of Monolith Catalytic Converters: A Two-Dimensional Reactor Model and the Effects of Radially Nonuniform Flow Distributions," *Chem. Eng. Sci.*, **44**, 2075 (1989).

Appendix: Derivation of the Heat-Transfer Coefficient

We shall show that for Eqs. 5 and 6 to yield the same Taylor-Aris dispersion as a full 2-D model, with the complete Poiseuille flow profile and radial solid temperature variation, the heat-transfer coefficient must be of the form in Eq. 2 for large γ. Specifically, we shall show that in the limit of infinite heat capacity ratio γ and thin wall thickness Δr, the appropriate heat-transfer coefficient which gives rise to the same effective diffusivity α_{eff} of the full problem corresponds to a tube with a constant heat flux at the wall. This result can be derived by the more conventional moments technique but is more conveniently derived by the recent Center Manifold formulation (Roberts, 1989).

We begin with steady heat transfer within a tube with constant wall flux q and laminar flow

$$2U\left(1-\frac{r^2}{a^2}\right)\frac{\partial T_g}{\partial x}=\alpha_g\frac{1}{r}\frac{\partial}{\partial r}\left(r\frac{\partial T_g}{\partial r}\right)$$

$$r\frac{\partial T_g}{\partial r}=0 \quad \text{at} \quad r=0$$

$$k_g\frac{\partial T_g}{\partial r}=q \quad \text{at} \quad r=a$$

$$T_g^b=\int_o^a T_g 2\left(1-\frac{r^2}{a^2}\right)2rdr$$

$$T_g^b=T_g^{\text{in}} \quad \text{at} \quad x=0 \tag{A1}$$

where we have defined the flow averaged bulk temperature T_g^b. It is a simple matter to show (Eagle and Ferguson, 1930) that $T_g^b-T_g(r=a)$ is independent of x and the effective heat-transfer coefficient is also independent of x

$$h=\frac{q}{T_g^b-T_g(r=a)}=\frac{24}{11}\left(\frac{k_g}{a}\right) \tag{A2}$$

which is the expression used in Eq. 2 in the limit of infinite γ. We note that if an isothermal condition was used at the wall, the effective heat-transfer coefficient would be different.

We now consider the case of effective diffusivity in a tube whose interphase heat transfer is described by a heat-transfer coefficient. This is equivalent to deriving α_{eff} of Eq. 14 for Eqs. 17 and 18 without the reaction term. The result has been obtained by the Center Manifold Theory in the text and by Balakotaiah and Chang (1994) earlier. It is simply Eq. 14

$$\alpha_{\text{eff}}=\left(\frac{\gamma^2}{1+\gamma}\right)U_{\text{eff}}^2\left[\frac{\pi a^2(\rho c_p)_g}{2\pi ah}\right] \tag{A3}$$

and substitution of Eq. A2 into Eq. A3 yields the effective diffusivity if indeed the constant-flux steady heat-transfer coefficient can be used.

Finally, we complete the argument by demonstrating that α_{eff} of the full problem can be represented by Eq. A3 with Eq. A2 in place in the limit of large γ and thin solid wall. We shall derive the results with the Center Manifold Theory. To obtain the same results as before, we use the tube radius a to scale the radial coordinate in the gas phase but use $a(\rho c_p)_g/2(\rho c_p)_s$ to scale the Cartesian coordinate in the solid phase. Using $(a^2\alpha_g)$ to scale time and $U(a^2/\alpha_g)$ to scale the axial coordinate, the governing equations become

$$\frac{\partial u}{\partial t}+2(1-r^2)\frac{\partial u}{\partial x}=\frac{1}{r}\frac{\partial}{\partial r}\left(r\frac{\partial u}{\partial r}\right) \tag{A4}$$

$$\frac{\partial v}{\partial t}=\frac{\lambda}{\gamma^2}\frac{\partial^2 v}{\partial y^2} \tag{A5}$$

$$r\frac{\partial u}{\partial r}\Big|_{r=0} = 0 \qquad \frac{\partial v}{\partial y}\Big|_{y=\gamma} = 0 \tag{A6}$$

$$u|_{r=1} = v|_{y=0} \tag{A7}$$

$$\frac{\partial u}{\partial r}\Big|_{r=1} = \frac{1}{2}\lambda\frac{\partial v}{\partial y}\Big|_{y=0} \tag{A8}$$

where γ is the heat capacity ratio and $\lambda = (a^2/\alpha_g)/(\Delta r^2/\alpha_s)$ is the ratio of the gas and solid diffusive times. A local Cartesian coordinate whose origin is at the inner wall has been imposed on the solid phase which is assumed to be thin. Axial diffusion has been neglected in both phases as before.

Equations A4 and A5 can be written as

$$\frac{\partial \boldsymbol{w}}{\partial t} = \mathfrak{L}\,\boldsymbol{w} - \boldsymbol{f}\frac{\partial u}{\partial x} \tag{A9}$$

where

$$\boldsymbol{w} = \begin{pmatrix} u \\ v \end{pmatrix}$$

$$\mathfrak{L} = \begin{pmatrix} \dfrac{1}{r}\dfrac{\partial}{\partial r}\left(r\dfrac{\partial}{\partial r}\cdot\right) & 0 \\ 0 & \dfrac{\lambda}{\gamma^2}\dfrac{\partial^2}{\partial y^2} \end{pmatrix}$$

$$\boldsymbol{f} = \begin{pmatrix} 2(1-r^2) \\ 0 \end{pmatrix}$$

We define the inner product

$$(w_1, w_2) = \frac{1}{1+\gamma}\left[2\int_0^1 u_1 u_2 r\,dr + \int_0^\gamma v_1 v_2\,dy\right] \tag{A10}$$

and the self-adjoint eigenvalue problem

$$\mathfrak{L}\boldsymbol{\phi}_i = \lambda_i \boldsymbol{\phi}_i \tag{A11}$$

whose eigenfunction satisfies the boundary conditions A6 to A8, we can expand $\boldsymbol{w}$ in terms of the eigenfunctions

$$\boldsymbol{w}(x,r,y,t) = \sum_{i=1}^{\infty} a_i(t,x)\boldsymbol{\phi}_i(r,y) \tag{A12}$$

We first note that the eigenvalue problem (A11) has a zero eigenvalue $\lambda_1 = 0$ with eigenfunction

$$\boldsymbol{\phi}_1 = \begin{pmatrix} 1 \\ 1 \end{pmatrix} \tag{A13}$$

such that $(\boldsymbol{\phi}_1, \boldsymbol{\phi}_1) = 1$. Substituting Eq. A12 into Eq. A4 and Eq. A5 and taking the inner product with respect to $\boldsymbol{\phi}_i$, one obtains the amplitude equation

$$\frac{\partial a_1}{\partial t} + \frac{1}{1+\gamma}\frac{\partial a_1}{\partial x} = -\sum_{i=2}^{\infty}(\boldsymbol{f}, \boldsymbol{\phi}_i)\frac{\partial a_i}{\partial x} \tag{A14}$$

$$\frac{\partial a_i}{\partial t} = \lambda_i a_i - (\boldsymbol{f}, \boldsymbol{\phi}_i)\frac{\partial a_1}{\partial x} \qquad i \neq 1 \tag{A15}$$

Since the operator $\mathfrak{L}$ is self-adjoint, all the eigenvalues are real. It is also easy to show that, except for λ_1, all other eigenvalues are negative. Hence, like the fast-decaying modes of Eq. 29, the modes a_i $(i = 2,\ldots)$ also decay rapidly and the system quickly approaches the zero mode a_1 whose gas and solid temperatures are in perfect thermal equilibrium as shown by the eigenfunction $\boldsymbol{\phi}_1$ of Eq. A13. Like Eq. 30, the adiabatic coupling of the decaying modes to a_1 gives rise to the effective dispersion and a quasi-steady analysis of Eq. A15 yields

$$a_i \sim \frac{(\boldsymbol{f}, \boldsymbol{\phi}_i)}{\lambda_i}\frac{\partial a_1}{\partial x} \tag{A16}$$

Upon substituting this into Eq. A14, one obtains:

$$\frac{\partial a_1}{\partial t} + \frac{1}{1+\gamma}\frac{\partial a_1}{\partial x} = \bar{\alpha}_{\text{eff}}\frac{\partial^2 a_1}{\partial x^2} \tag{A17}$$

where

$$\bar{\alpha}_{\text{eff}} = \sum_{i=2}^{\infty}\frac{(\boldsymbol{f}, \boldsymbol{\phi}_i)^2}{|\lambda_i|} \tag{A18}$$

is the dimensionless effective diffusivity.

Rather tedious algebra is necessary to compute the eigenfunctions $\boldsymbol{\phi}_i$ and the eigenvalues λ_i. When substituted into Eq. A18, the finite series can be shown to converge to a closed-form limit. We shall omit the details here and simply state the result. The effective equation for T_g is

$$\frac{\partial T_g}{\partial t} + U_{\text{eff}}\frac{\partial T_g}{\partial x} = \alpha_{\text{eff}}\frac{\partial^2 T_g}{\partial x^2} \tag{A19}$$

where

$$U_{\text{eff}} = \frac{U}{1+\gamma} \tag{A20}$$

$$\alpha_{\text{eff}} = \frac{U^2 a^2}{\alpha_g}\left[\frac{1}{3}\frac{\gamma/\lambda}{(1+\gamma)^3} + \frac{1}{48}\frac{(1+6\gamma+11\gamma^2)}{(1+\gamma)^3}\right] \tag{A21}$$

It is interesting to note that α_{eff} is simply the sum of the $\lambda \to 0$ and $\lambda \to \infty$ limits, viz. fast diffusion in gas and solid limits respectively. It is clear Eq. A19 agrees with Eq. 10 as is expected for any chromatographic thermal wave speed. It is less obvious that as Δr approaches zero, viz. λ approaches infinity, and γ approaches infinity, Eq. A21 indicates that dispersion is due mainly to slow gas-phase radial diffusion which is responsible for the imperfect solid-gas thermal communication

$$\alpha_{\text{eff}} \sim \frac{11}{48}\left(\frac{U^2 a^2}{\alpha_g}\right)\frac{1}{\gamma} \tag{A22}$$

This expansion is in agreement with Eq. A3 in the limit of large γ and when Eq. A2 and Eq. A20 have been substituted. We have hence shown that, in the limit of small Δr (large λ) and large γ, the effective thermal diffusivity in a cylinder can be obtained by using a radially lumped model whose gas-solid heat-transfer coefficient is obtained from a steady, constant-flux formulation. This is a rather unintuitive result which required a detailed analysis. How the eigenfunctions ϕ_i can be obtained using the formulation of Roberts (1989) and the summation of the series in Eq. A18 can be found in Balakotaiah and Chang (1995).

Manuscript received Apr. 13, 1994, and revision received Sept. 19, 1994.